Int. J. Electrochem. Sci., 16 **(2021)** Article ID: 210562, doi: 10.20964/2021.05.32

International Journal of
ELECTROCHEMICAL
SCIENCE
www.electrochemsci.org

Microstructure and Properties of ZrO_2 Alloyed Layer on Ti-6Al-4V

Meili Ban[1,], Kunda Li[1], Qingshuang Tao[1], Ailan Fan[1,*], Bin Tang[1], Jianqiang Zhang[2]*

[1] College of Materials Science and Engineering, Taiyuan University of Technology, Taiyuan 030024, PR China.
[2] Shanxi Institute of Energy，Jinzhong030600，PR China
[*]E-mail: fanailan@tyut.edu.cn; banmeili@qq.com

Received: 20 November 2020 / *Accepted:* 7 January 2021 / *Published:* 31 March 2021

In this paper, the uniform and dense Zr alloyed layer was prepared on Ti-6Al-4V (TC4) alloy by double glow plasma surface alloying technology, and subsequently the Zr alloyed layer was oxidized by MP-CVD technology to form a uniform and dense ZrO_2 alloyed layer. The purpose is to improve the corrosion resistance and wear resistance of TC4 alloy. To evaluate the wear performance of the ZrO_2 alloyed layer, the specimens were measured by wear scars profile curves and friction coefficient curve in human simulated saliva. Then, the open circuit potential method and the potentiodynamic polarization method were used to determine the corrosion performance of the ZrO_2 alloyed layer in human simulated simulated saliva. Finally, the surface and cross section morphology and phase composition of the zirconium oxide coating were analyzed The results indicate that the ZrO_2 alloyed layer exhibits striking low friction coefficient, very narrow wear scar profile and high self-corrosion current, showing the excellent wear resistance and corrosion resistance.

Keywords: Ti-6Al-4V; ZrO_2 alloyed layer; Wear resistance; Corrosion resistance

1. INTRODUCTION

Due to its non-toxic, high strength, light weight, excellent biocompatibility and corrosion resistance, titanium and titanium alloys, especially Ti6Al4V (TC4), have been widely used in many fields such as biomedical, chemical, energy and aerospace industries [1-4]. It is generally believed that the main reason of the better corrosion resistance and biocompatibility of titanium and titanium alloys is its automatically formed a TiO_2 passive film in air [5,6]. However, in the environment containing Cl^- [7], the TiO_2 passive film would be fallen off, resulting in poor corrosion resistance. On the other hand, the poor friction and wear resistance of titanium alloys also affects the safety and reliability of titanium alloys, and limits its application. For these reasons, people need to seek surface modification

process of titanium material to improve their surface properties. Some researchers modified TC4 using a ceramic layer by surface modification technology. Ceramic layer may act as a protective barrier between the metal and the hostile environment to improve the corrosion resistance and wear properties [8].

To date, the common various surface coating techniques of titanium material include micro-plasma oxidation (MPO) technique [9]，laser treatment [10], chemical vapor deposition [11], physical vapor deposition [12] and ion implantation [13] and double glow plasma surface alloying and so on. The double glow plasma surface alloying technology has been considered one of more effective methods owing to its high percolation speed, good film bonding force, controllable film thickness and energy conservation. At present, the double glow plasma surface alloying method has been applied to modified titanium alloys for improvising the alloy's properties [14].

Recent studies have reported that Zr has been considered as a nontoxic and no allergic element. Due to Zr and Ti are located in the same main group in periodic table of elements, it exhibits same extra nuclear electronic structure and lattice type as Ti [15]. Zr also has the same good overall properties as Ti [16,17]. Previous researches have shown that the addition of Zr element to Ti alloys makes better the wear and corrosion resistance [18-21]. For example, Mi-Kyung Han and Moon-Jin Hwang [22] has studied that the addition of Zr element exhibited better corrosion resistance compared to that of Ti. ZrO_2 have been widely concerned and studied for their advantages such as excellent mechanical properties and good biocompatibility [23]. It provides the best choice for improving the wear and corrosion resistance of TC4 alloy. In this study, a new duplex-treatment technology merging double glow plasma surface alloying technology with microwave plasma chemical vapor deposition (MP-CVD) has been exploited to prepare the ZrO_2 alloyed layer [24]. First of all, Zr alloyed layer was made ready by double glow plasma surface alloying technology on TC4, then ZrO_2 alloyed layer was formed by the Zr layer is oxidized utilizing MP-CVD technology. These experiments mainly studies the surface morphology, microstructure, corrosion resistance and wear resistance of the ZrO_2 alloyed layer on TC4, and compares it with the relevant properties of the TC4 substrate.

2. EXPERIMENT MATERIALS AND METHODS

2.1. Preparation of ZrO_2 alloyed layer

TC4 alloys with 15 mm in diameter and 3.5 mm thickness were used as the substrate. The nominal component of TC4 alloy in wt. % is: 6.8 Al，4.2 V，0.07 Si，0.10 Fe，0.03 C，0.14 O，0.015N，0.003H and the balance Ti. The TC4 substrates were successively ground with a series of SiC sand paper and polished to mirror finish, then respectively ultrasonic cleaned in deionized water, acetone and ethanol, and naturally dried in the cool air.

A pure Zr plate with a purity of 99.9% and a size of 55 mm × 55 mm × 5 mm was used as the source target of zirconium. The preparation of a Zr alloyed layer was carried out in a double glow plasma surface alloying technology. The optimized processing parameters were as follows: substrate temperature = 800 °C, treatment time = 2h, working pressure = 35 Pa, difference between the target

electrode voltage and substrate voltage = 250 V, target distance = 15mm. Subsequently, the zirconium-treated sample was oxidized at 650 ° C for 30 minutes to form ZrO_2 alloyed layer in plasma chemical vapor deposition (MPCVD) in which the oxygen flux was 5.sccm.

2.2. Samples characterization

The surface and cross-sectional morphology of ZrO_2 alloyed layer was detected by a field-emission scanning electron microscopy (FEI Nano-SEM 430). The dispensation of elements the ZrO_2 alloyed layer was examined by energy-dispersive X-ray spectroscopy (EDS, QX200, Bruker). The phase composition of every sample was observed by X-ray diffraction (XRD, DX-2700, and Haoyuan) with Cu Kα radiation.

2.3. Electrochemical measurements

The electrochemical corrosion was measured by Princeton PMC-2000 electrochemical workstation using a three-electrode system in simulated saliva. The reference electrode and auxiliary electrode were saturated calomel electrode and a platinum electrode, respectively. The electrode made of sample was the working electrode. The measurement of open-circuit potential (OCP) was immersed into the solution for 1800s. Subsequently, the potentiodynamic polarization curve was conducted in the 37℃ temperature at a scanning rate of 0.5 mV/s, its scanning potential was set as from -1.5V to 1.5V.

2.4. Wear resistance

The wear resistance of TC4 substrate and ZrO_2 alloyed layer were tested by MFT-R4000 reciprocating friction and wear tester in the natural environment temperature and simulated saliva. All samples were friction to and fro using the friction Pairs of Si_3N_4 ceramic ball with a 5 mm diameter under a normal load of 5 N at a frequency of 2 Hz and an ambient temperature of 25 ℃ for 30 minutes. The surface morphology of wear scar TC4 titanium substrate and ZrO_2 alloyed layer were examined by WIVS white light interference profilometer.

3. RESULTS AND DISCUSSION

3.1. Materials characterization

Fig.1. shows the surface morphology of TC4 substrate and ZrO_2 alloyed layer on TC4. The untreated TC4 substrate has a smooth surface and slight indentation scratches, as shown in the Fig.1.(a). As a whole, the ZrO_2 alloyed layer exhibited dense, homogeneous surface without defects of porosity and cracks (Fig.1b). The ZrO_2 alloyed layer has continuous pits on the surface, which may be attributed to the formation of continuous solid solution between the TC4 with Zr during surface

alloying process. In addition, the Zr targets is heated to high temperature by bombardment of the plasma, which at the same time causes a large number of crystal defects on the work piece surface, and the increase of surface roughness after oxidation.

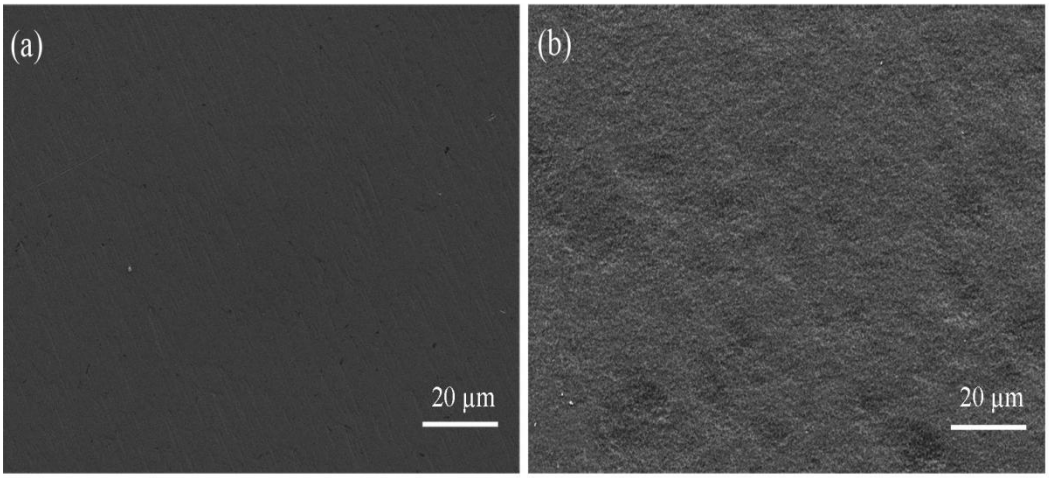

Figure 1. The surface morphology of (a) TC4 and (b) ZrO_2 alloyed layer.

Fig.2. presents the XRD spectrum of TC4 substrate and ZrO_2 alloyed layer. According to the literature[25-27], the peaks of ZrO_2 phase are mainly distributed in 2θ=28.23°、30.30°、35.41°、50.42°、61°、74.78°. The surface of Zr -TC4 alloyed layer after oxidation is primarily composed of metallic ZrO_2 phase. This demonstrates that ZrO_2 was successfully deposited on the surface of TC4. The presence of ZrO_2 phase makes the coating have higher hardness, wear resistance and corrosion resistance than that of TC4.

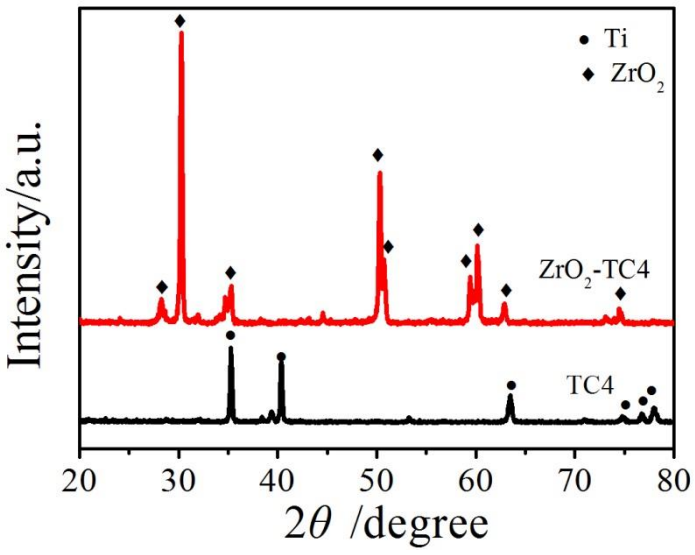

Figure 2. XRD spectrum of TC4 and ZrO_2 alloyed layer.

The cross-sectional morphology and corresponding EDS elemental maps of the ZrO_2 alloyed layer are shown by Fig.3. The thickness of ZrO_2 alloyed layer is composed of 6.2μm ZrO_2 deposited layer and 10.6μm diffusion layer. The reason of diffusion layer formation may be that a certain amount of Zr elements are deposited on the surface of the TC4 alloy as the sputtering progresses, the Zr diffuses into the substrate under the effect of the concentration gradient and temperature. However, the sedimentary layer will be formed when the deposition rate is greater than the diffusion rate. Combined with the EDS elemental maps, the alloyed layer is mainly consisted of O and Zr elements. This indicates that a part of the diffusion layer is also oxidized.

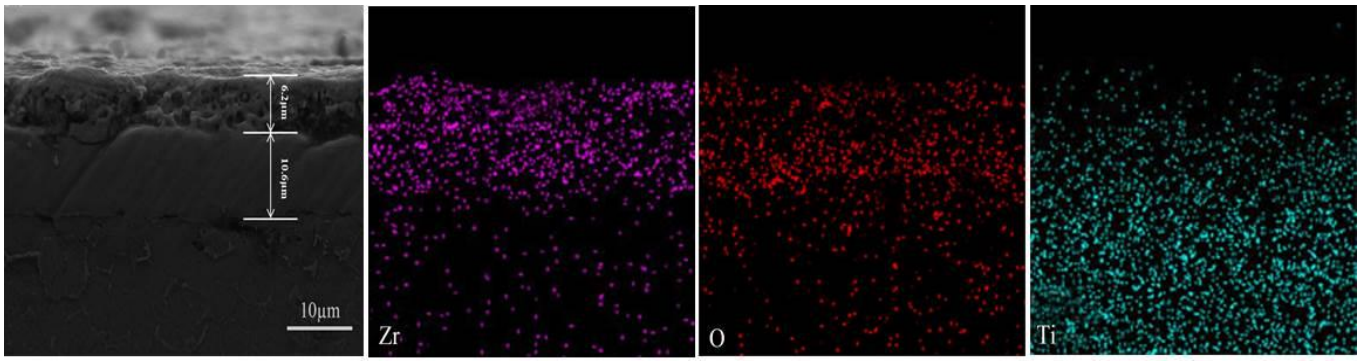

Figure 3. The cross-sectional morphology and corresponding EDS elemental maps of ZrO_2 alloyed layer.

3.2. Corrosion behavior

Fig. 4(a) shows the open circuit potential (OCP) as a function of dipping time for TC4 and ZrO_2 alloyed layer in simulated saliva at 37℃ temperature. The sample was immersed in the solution, the initial OCP of the untreated sample is 0.102V. As the increase of immersion time, the OCP has been decreasing. It indicated that TC4 substrate is prone to corrode because metal surface fails to absorb oxygen to form TiO_2 film, which implies that there is no barrier layer on the surface of the substrate to prevent electron transfer at the electrode-electrolyte interface , it cannot protects the material and obtain a stable OCP value[5,22]. The initial OCP of ZrO_2 alloyed layer is 0.13V, then slowly declines for some time, after more than 600 seconds, the OCP curves gradually began to stabilize and reach a relatively stable value around 0.114V. At the beginning of this process, the reason for the first drop in voltage may be ZrO_2 alloyed layer is prone to corrode due to surface roughness and structure defects of oxide. In addition, the transfer of diffusion reactants may be controlled due to the presence of unoxidized Zr particles in ZrO_2 alloyed layer, so the contact and reaction between the reactants take a long time, therefore high the OCP value and little anodic dissolution current at the beginning; As time goes by, the reactants gradually contact and react with each other, so the OCP value decreases and thus anodic dissolution current increases [28-30]. When the corrosion resistance of the ZrO_2 alloyed layer reached a relatively stable value, the anodic dissolution current and the OCP

value also reached a stable value. Compared with the untreated TC4, the ZrO_2 alloyed layer significantly improve the OCP value of TC4, and corrosion trend becomes smaller and shows the ZrO_2 alloyed layer has better thermodynamics stability, which is due to a uniform and dense oxide film formed on the substrate surface.

Fig.4. (b) is potentiodynamic polarization curves of ZrO_2 alloyed layer and untreated TC4 in simulated saliva. The curves of ZrO_2 alloyed layer is positively shifted compared to the TC4 substrate，which is possibly due to the increase of the cathode current and the reduction of the anode dissolution current, the solution forms an adsorption barrier on the surface of the film, blocking the corrosion of the coating by the solution ions [30, 31]. In addition, two corrosion curves are passivized. The passivation zone of the ZrO_2 alloyed layer starts at around -450 mV, while the passivation zone of the TC4 substrate starts at around-480 mV. The passivation current density of ZrO_2 alloyed layer is about an order of magnitude smaller than that of the substrate. The smaller the passivation current density and the lower the corrosion rate in the passivized state indicate that ZrO_2 alloyed layer is easy to passives, the passivation film is formed earlier than the TC4 substrate, and its corrosion resistance is higher than that of the TC4 substrate. The ZrO_2 alloyed layer improves corrosion resistance properties of the TC4 substrate from the viewpoint of corrosion dynamics. According to these potentiodynamic polarization curves, corrosion potential (Ecorr) , corrosion current density (Icorr) and corrosion rate of all samples are obtained via the Tafel method [32] and then the calculated results are shown in Table 1. The Table 1 data showed the self-corrosion potential (E_{corr})) of the alloyed layer sample is higher than that of TC4 substrate, and self-corrosion current density (I_{corr}) of the alloyed layer sample is almost 10 times lower than that of TC4 substrate, especially the corrosion rate for the alloyed layer sample is almost 20 times lower than that of TC4 substrate. Renu Kumari, et al. [33] reported that the corrosion rate decreases is possibly attributed to the transformation of the crystalline phase, microstructural homogenization and reduction in porosity. The self-corrosion potential (E_{corr}) and self-corrosion current density (I_{corr}) indicates the thermodynamic trend of the corrosion process. The higher the potential and the smaller the current density show the better the corrosion resistance. Thus the ZrO_2 alloyed layer significantly improves the corrosion resistance of TC4 in human simulated saliva.

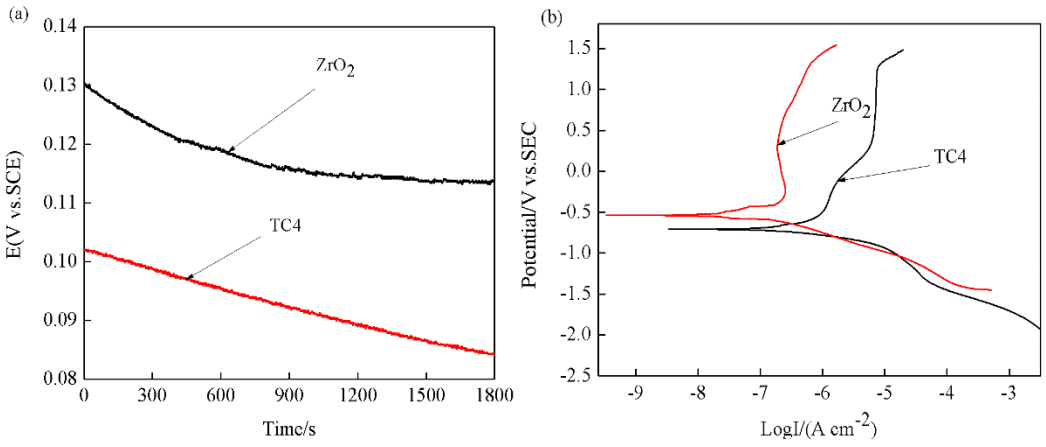

Figure 4. The open circuit potential and potentiodynamic polarization curves of TC4 and ZrO_2 alloyed layer in human simulated saliva (a) The OCP curve of TC4 and ZrO_2 alloyed layer (b) The potentiodynamic polarization curve of TC4 and ZrO_2 alloyed layer

Table 1. Electrochemical parameters obtained from potentiodynamic polarization curves of specimens in human simulated saliva

Samples	E_{corr}/mV	I_{corr}/(A•cm^{-2})	Corrosion Rate/(10^{-2}mm•a^{-1})
TC4	-708.3	2.43×10^{-7}	1.06×10^{-3}
TC4-ZrO_2	-538.26	2.52×10^{-8}	2.12×10^{-4}

3.3. Wear resistance

Fig.5. shows friction coefficient curves, wear scars profile curves and corresponding surface morphology of TC4 substrate and ZrO_2 alloyed layer in human simulated saliva. As you can see from Fig.5 (a), during the rubbing process, the friction coefficient of TC4 substrate fluctuates within 0.1 and 0.16, and is almost in a stable state. The friction coefficient value is at a steady state in the presence of simulated saliva, which is consistent with the previously reported results [34]. A certain running-in period is required at the beginning of friction due to the roughness and average grain size of the ZrO_2 alloyed layer surface, which will produce abrasive cutting and plugging effects on the sharp surface roughness [34]. The friction coefficient of the ZrO_2 alloyed layer increases sharply at first, and then reaches a constant 0.4 after 2 min. The friction coefficient not only reflects the size of the load and the friction speed, but also is related to the plowing effect of the material's surface morphology，contact form, and surface roughness. Compared with TC4 substrate, the friction coefficient of the ZrO_2 alloyed layer is obviously higher than that of the TC4 substrate. The reason may be that the surface roughness of the ZrO_2 alloy layer is higher than that of TC4.

Fig.5. (b) is the wear scar profiles. The wear scar depths of TC4 substrate and ZrO_2 alloyed layer are 24.21 μm and 3.14 μm, respectively, and the wear scar widths are 0.851 mm and 0.31 mm, respectively. The wear volume (Wv) TC4 and ZrO_2 alloyed layer can be calculated as 68.7×10^{-3} mm^3 and 3.2×10^{-3}mm^3, respectively. The wear rate of TC4 and ZrO2 alloyed layer are 2.748 mm^3•N^{-1}•m^{-1} and 0.128 mm^3 • N^{-1} • m^{-1}, respectively. The rate of wear of the ZrO_2 alloyed layer is smaller compared with TC4, which is due to the high hardness of ZrO_2. The presences of ZrO2 also decrease its wear rate according to Yehia, Hossam M. et al. [35] in simulated saliva. This indicates that ZrO_2 alloyed layer exhibits better wear resistance than TC4 substrate.

Fig.5 (c) and Fig.5 (d) shows corresponding wear morphology of TC4 substrate and ZrO2 alloyed layer under different magnifications. It can be observed from Figure (c), the wear surface of the TC4 substrate are many furrows and there are a lot of spalling pits in the grooves, serious laminar tear phenomenon and plastic deformation occurred. This is because the hardness of the ceramic ball is higher than the substrate, so the contact area between the sample and the friction pair become larger, ceramic balls will have a great plowing effect on the surface of the TC4 substrate under the action of the loading force, which occur the surface plastic deformation and grooving [36]. Subsequently, after the reciprocating friction of 30 minutes, it is found that the near area of spalling pits was more severely worn on the surface of the substrate. Therefore, the surface wear mechanisms of TC4 substrate include abrasive wear and adhesive wear. Compared with the dry friction done before [24], there is almost no

large amount of wear debris, deep ridges and grooves on the surface of the TC4 substrate due to the lubrication effect of simulated saliva.

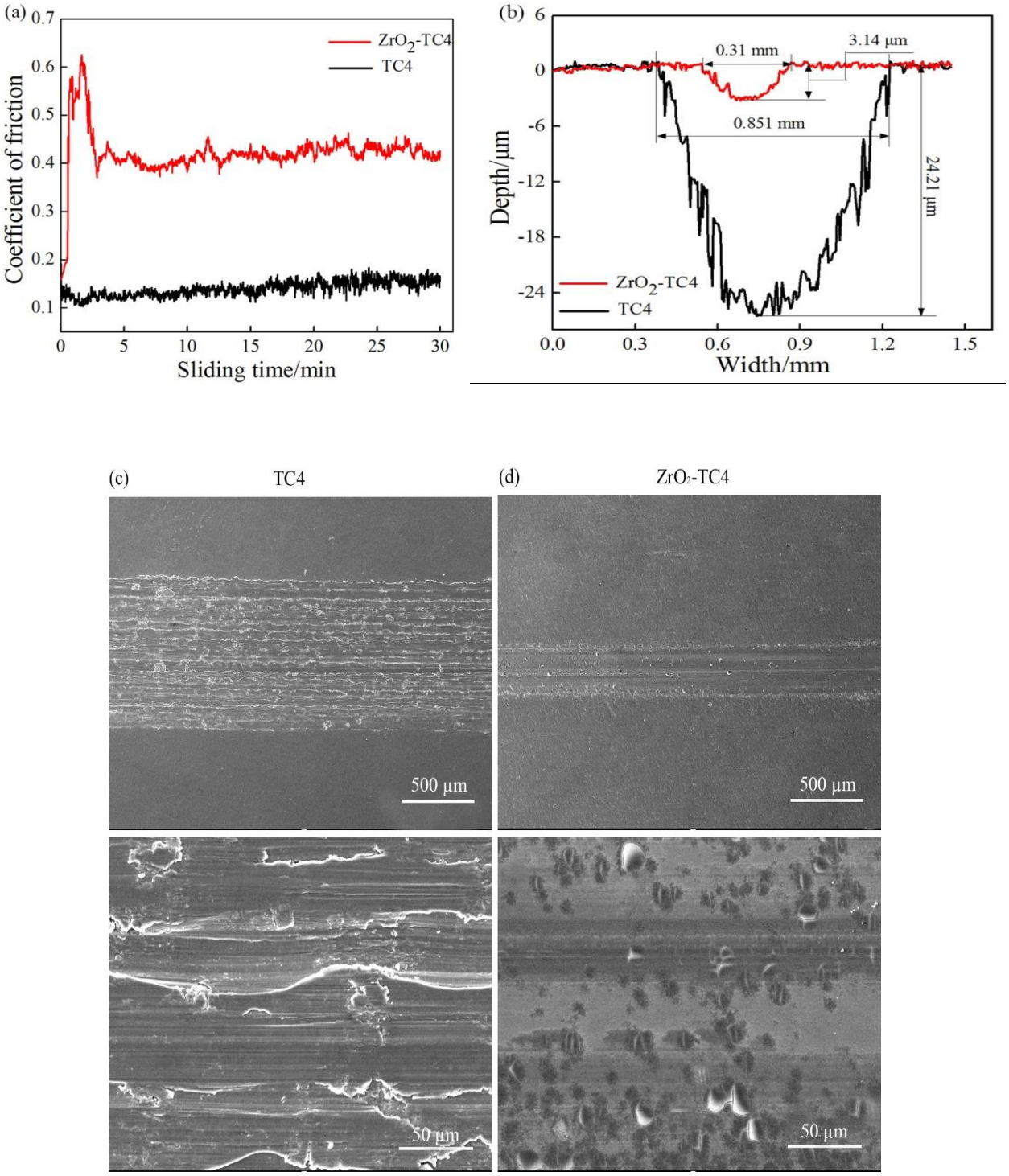

Figure 5. The friction coefficient curve, wear scar profile and surface topography of TC4 and ZrO_2 alloyed layer (a) Friction coefficient curve (b) Wear scar profile (c) surface topography of TC4 (d) Surface topography of ZrO_2 alloyed layer

The wear surface of ZrO_2 alloyed layer is no obvious furrows and ridges with a few abrasive particles existed, and only a small amount of wear and a small amount of plastic deformation occurred on the coating surface. Meanwhile, the worn surface has white shell-like protrusions and a part of slight pits in the wear marks. This is because Si_3N_4 ball and ZrO_2 alloyed layer are ceramic materials with high hardness, and adhesive wear will not occur between the two ceramic materials [37]. In addition, the outstanding part of the surface of the ZrO_2 alloy layer preferentially contacts the grinding ball under the action of load; some protrusions may be not flattened after a long period of friction. The main wear mechanism of ZrO_2 alloy layer is abrasive wear. Compared with the substrate, the wear width of ZrO_2 alloyed layer (Fig.5 (d)) is relatively narrow and smooth. This may be due to the increase of surface hardness and the lubrication effect of solution. Thus, according to the friction coefficient curve, wear scar profile and wear scar morphology, the wear resistance of ZrO_2 alloyed layer is distinctly better than TC4 itself.

4. CONCLUSIONS

A uniform and dense ZrO_2 alloyed layers were successfully prepared on the surface of TC4 alloy by double glow plasma metallization and MP-CVD technology. The cross-section thickness of ZrO_2 alloyed layers is about 18.8 μm. The alloy layer is divided into a deposited layer and a transition layer. It mainly consists of the ceramic phase of ZrO_2. The ZrO_2 alloyed layer greatly improves the corrosion resistance and wear resistance of TC4 alloy in simulated saliva.

ACKNOWLEDGEMENT
This work was supported by the National Natural Science Foundation of China (51671140, 51474154) and Project of Shanxi Science Association.

References

1. L. J. Zhang, X.Y. Wang, Q.Y. Guo, T. Xie, X.Y, Xiang and H, Chang, *Aeronautical Manufacturing Technology*, 16 (2013) 129.
2. A.M. Fekry and R.M. El-Sherif, *Electrochimi. Acta*, 54 (2009) 7280.
3. G.T. Burstein and C. Liu, *Corros. Sci.,* 49 (2007) 4296.
4. J. Fojt, L. Joska and J. Málek, *Corros. Sci.,* 71 (2013) 78.
5. J.F. Li, X.Y. He, G.N. Zhang, R.Q. Hang, X.B. Huang, B. Tang and X.Y Zhang, *Bioelectrochem.,* 121 (2018) 105.
6. V.A. Alves, R.Q. Reis, I.C.B. Santos, D.G. Souza, T.D.F. Gonalves, M.A. Pereira-Da-Silva, A. Rossi and L.A.D. Silva, *Corros. Ence.,* 51 (2009) 2473.
7. J.J. de Damborenea, M.A. Arenas, M.A. Larosa, A.L. Jardini, C.A. de Carvalho Zavaglia and A. Conde, *Applied Surf. Sci.,* 393 (2017) 340.
8. M. Chellappa and U. Vijayalakshm, *J. Asian Ceram. Soc.,* 5 (2017) 326.
9. Z.P. Yao, Z.H. Jiang, X.T. Sun, X.G. Xin and Y.P. Li, *Thin Solid Films*, 468 (2004) 120.
10. R.S. Razavi, M. Salehi, M. Monirvaghefi and G.R. Gordani, *J. Mater. Process. Tech.,* 203 (2008) 315.

11. D.H. Kuo and K.W. Huang, *Surf. Coat. Technol.,* 135 (2001) 150.
12. M. Khaled, B.S. Yilbas and J. Shirokoff, *Surf. Coat. Technol.,* 148 (2001) 46.
13. L. Thair, U. KamachiMudali, N. Bhuvaneswaran, K.G.M. Nair, R. Asokamani and B. Raj, *Corros. Sci.,* 44 (2002) 2439.
14. S. Rossi, L. Fedrizzi, T. Bacci and G. Pradelli, *Corros. Ence.,* 45 (2003) 511.
15. C.Q. Xia, Z.G. Zhang and Z.H. Feng, *Corros. Sci.,* 112 (2016) 687.
16. Y. Okazaki, S. Rao and T. Tateishi, *Mater. Sci. Eng., A*, 243 (1998) 250.
17. M. Niinomi, *Biomater.,* 24 (2003) 2673.
18. X.Y. Zhang, G.N. Zhang, J.F. Li, X.J. He, Y.Y. Wang, R.Q. Hang, X.B. Huang and B. Tang, *Mater. Sci. Eng., C,* 90 (2018) 523.
19. D.R.N. Correa, F.B. Vicente, T.A.G. Donato, V.E. Arana-Chavez, M.A.R. Buzalaf and C.R. Grandini, *Mater. Sci. Eng., C*, 34 (2014) 354.
20. W.F. Ho, W.K. Chen, S.C. Wu and H.C. Hsu, *J. Mater. Sci. Mater. Med.,* 19 (2008) 3179.
21. H.C. Hsu, S.C. Wu, Y.C. Sung and W.F. Ho, *J. Alloys Compd.,* 488 (2009) 279.
22. M.K. Han, M.J. Hwang, M.S. Yang, H.S. Yang, H.J. Song and Y.J. Park, *Mater. Sci. Eng., A,* 616 (2014) 268.
23. F. Chen, H. Zhu, J.M. Wu, S. Chen and J. Xiao, *Ceram. Int.,* 46 (2020) 11268.
24. Q.S. Tao, M.L. Ban, S.W. Yu, A.L. Fan and B. Tang, *Heat Treatment of Metals*, 44 (2019) 58.
25. Y.H. Cui, Z.C. Hu, Y. D. Ma, Y. Yang, C.C. Zhao and Y. T. Ran, *Surf. Coat. Technol.,* 363 (2019) 112.
26. K. Prabakar, A. Park, N. Cho, W.I. Lee, C.K. Hwangbo, J.G. Lee and C. Lee, *Vac.,* 82 (2008) 1367.
27. H.Y. Wu, Y. LI, Y. Wang, P.Z. Zhang and W.F. Rao, *J. Rare Earths*, 34 (2016) 958.
28. R.Q. Hang, X.B. Huang, L.H. Tian and Z.Y. He, Electrochimi. Acta, 70 (2012) 382.
29. R.Q. Hang, S.L. Ma, V. Ji and P.K. Chu, Electrochim. Acta, 55 (2010) 5551.
30. X.L.Cheng, S.G. Roscoe, *Biomater.,* 26(2005)7350.
31. H.L. Liu, Z.P. Tong, W.F. Zhou, Y. Yang, J.F. Jiao and X.D. Ren, *J. Alloys Compd.,* 846 (2020) 155837.
32. C.L. Liu, Y.C. Xin and P.K. Chu, *J. Mater. Res.,* 22 (2007) 1806.
33. R. Kumari and J.D. Majumdar, *Appl. Surf. Sci.,* 420 (2017) 935.
34. J.Q. Wang, J. Zhou, H.Y. Long, Y.N. Xie, X.W. Zhang, H. Luo, Z.J. Deng, Q.P. Wei and Z.M. Yu, *Surf. Coat. Technol.,* 258 (2014) 1032.
35. H.M. Yehia, A. El-Tantawy, I.M. Ghayad, A.S. Eldesoky and O. El-kady, *J. Mater. Res. Technol.,* 9 (2020) 8820.
36. X.M. Sui, J. Lu, and W.P. Zhang, *J. Therm. Spray Tech.,* 29 (2020) 510.
37. I. Cvijović-Alagić, Z. Cvijović, S. Mitrović, V. Panićet and M. Rakin, *Corros. Sci.,* 53 (2011) 796.